Light: Science & Applications (2013) 2, e72; doi:10.1038/lsa.2013.28

www.nature.com/lsa

ORIGINAL ARTICLE

Ultra-thin, planar, Babinet-inverted plasmonic metalenses

Xingjie Ni, Satoshi Ishii, Alexander V Kildishev, and Vladimir M Shalaev

We experimentally demonstrate the focusing of visible light with ultra-thin, planar metasurfaces made of concentrically perforated, 30-nm-thick gold films. The perforated nano-voids—Babinet-inverted (complementary) nano-antennas—create discrete phase shifts and form a desired wavefront of cross-polarized, scattered light. The signal-to-noise ratio in our complementary nano-antenna design is at least one order of magnitude higher than in previous metallic nano-antenna designs. We first study our proof-of-concept 'metalens' with extremely strong focusing ability: focusing at a distance of only 2.5 μm is achieved experimentally with a 4-μm-diameter lens for light at a wavelength of 676 nm. We then extend our work with one of these 'metalenses' and achieve a wavelength-controllable focal length. Optical characterization of the lens confirms that switching the incident wavelength from 676 to 476 nm changes the focal length from 7 to 10 μm, which opens up new opportunities for tuning and spatially separating light at different wavelengths within small, micrometer-scale areas. All the proposed designs can be embedded on-chip or at the end of an optical fiber. The designs also all work for two orthogonal, linear polarizations of incident light.
Light: Science & Applications (2013) **2,** e72; doi:10.1038/lsa.2013.28; published online 26 April 2013

Keywords: metalens; nano-antennas; plasmonics; wavefront shaping

INTRODUCTION

The convergence or divergence of an optical beam in a traditional, refraction-based lens depends on the phase change of the light propagating inside the lens. The strength of the light bending in such a system is therefore limited by the refractive index of a given dielectric. Fabrication challenges are also paramount, as it is very difficult to make lenses with a large aperture and a short focal length. By using the Fresnel lens design, the mass and volume of material can be reduced, but the thickness of the lens is still on the wavelength scale. Fresnel zone plates, which consist of concentric rings (Fresnel zones) and use diffraction instead of refraction or reflection, also can be used to focus light, but it is impossible to shrink the size down to only a few wavelengths since the radius differences between the neighboring opaque and transparent rings must be at least half of the wavelength of the incident light, and typically a large number of rings is required for good performance. However, advances in the area of plasmonics have now opened up a new era for building compact, planar lenses. A number of plasmonic lenses have been developed recently based on superoscillation[1,2] and mode-index manipulation of guided waves inside nano-apertures (slits or holes).[3–6] Nevertheless, those designs suffer from limited phase control, which restricts their minimum sizes and thicknesses: either the size of the lens cannot be further reduced because the design is based on the diffraction of the light through transparent/opaque regions, or the thickness of the lens must be comparable to the operational wavelength because the phase change is obtained by light propagating inside the lens material.

In the last few years, subwavelength-sized plasmonic nano-antennas on a planar surface have been shown to create phase shifts covering the full range (from 0 to 2π) in cross-polarized scattered light due to their asymmetric plasmonic resonances.[7–14] An array of such nano-antennas can form a metasurface to bend the light abnormally[7,8] in a fairly broad range of wavelengths and can create, for example, an optical vortex beam.[7,12] In addition, a metasurface arranged of plasmonic nano-antennas can be used as a very efficient coupler between propagating waves and surface waves.[10]

These phase-shifting, plasmonic nano-antennas also can be used to build optical lenses with surprising properties.[15–17] During the preparation of this paper, a conceptual device was proposed independently in the near-infrared (near-IR) spectral range.[18] However, in contrast to conventional nano-antennas shown in Refs. 8 and 18, in this paper, we use an inverted design built on Babinet's principle, i.e., instead of metallic nano-antennas we use a set of similarly shaped nano-voids (Babinet-inverted, or complementary nano-antennas) milled in a thin metallic film, which provides a significantly higher signal-to-noise ratio. We then arrange the nano-voids in concentric arrays to create a planar plasmonic metalens and to experimentally demonstrate efficient focusing of the incident light. In contrast to the near-IR lens with focusing distances on the cm scale discussed in Ref. 18, our plasmonic metalenses are very small in size (a few micrometers) and have an extremely strong focusing ability, with focal lengths of only few micrometers. Our metalenses also work across the entire visible spectral range and can spatially

School of Electrical and Computer Engineering and Birck Nanotechnology Center, Purdue University, West Lafayette, IN 47907, USA
Correspondence: Professor VM Shalaev, School of Electrical and Computer Engineering and Birck Nanotechnology Center, Purdue University, West Lafayette, IN 47907, USA
E-mail: shalaev@purdue.edu
Received 6 September 2012; revised 15 January 2013; accepted 7 February 2013

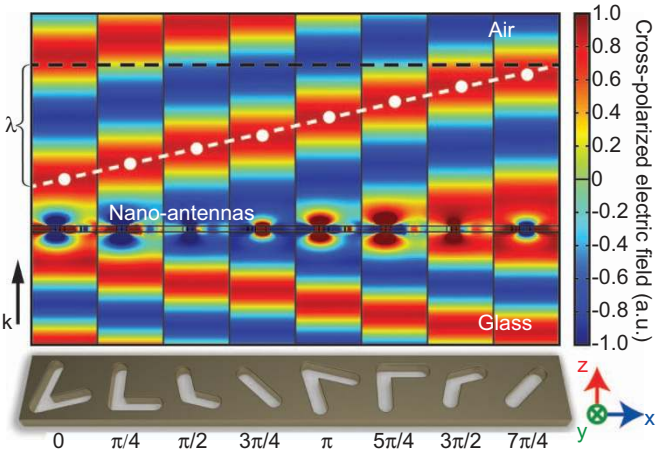

Figure 1 Schematic designs and the results of full-wave simulations of the individual Babinet-inverted nano-antennas at a wavelength of 676 nm. The nano-antennas create discrete phase shifts from 0 to $7\pi/4$ for cross-polarized light. The linearly-polarized light enters the system from the glass substrate side of the sample. The pseudo-color field map indicates the cross-polarized light scattered from each nano-antenna, clearly revealing the discrete phase shifts.

separate light at different wavelengths within small, micrometer-scale areas.

METHODS

Our metalenses are comprised of an array of different shapes of nano-voids in a thin metallic film. Each shape of the complementary nano-antennas provides a specific, discrete phase shift to the cross-polarized scattered light (that is, the scattered polarization is perpendicular to the incident polarization). The shapes are designed by simulating each kind of nano-antenna individually using full-wave, three-dimensional, finite element method calculations. Figure 1 shows the phase shift ranging from 0 to $7\pi/4$ within the visible range depending on the nano-antenna design. By using the complementary design, we increase the ratio of the transmitted power of the useful, focused cross-polarized light (P_s) to the transmitted power of the background, co-polarized scattered light (P_n), which is equivalent to increasing the overall signal-to-noise ratio (SNR$=10\log_{10}(P_s/P_n)$ dB) of the design. In essence, the SNR in our case is quite similar to the polarization extinction ratio often used to characterize 90° phase plates. Our design efficiently prevents the transmission of the co-polarized component because the rest of the sample is opaque. The SNR in our design is estimated using two-dimensional arrays in the simulation. For a reasonable periodicity of 300 nm in both the x and y directions, the SNR for the original metallic nano-antenna design[8] at 1.5 μm is about −14 dB, while for the Babinet-inverted design at 676 nm the SNR is about −3 dB, which is 11 dB higher.

We arrange the nano-antennas in concentric rings as illustrated in Figure 2a. The nano-antennas of different shapes are distributed in such a way that the individual, discrete phase shifts created by each nano-antenna element cause the overall cross-polarized wave front scattered at the interface to focus at a focal distance f. The design of the metalens is obtained through the reciprocity principle, i.e., by reverse-propagating the light from a point source located at the focal point back to the lens plane. Therefore, the required relative phase shift φ for a nano-antenna located at a distance of r from the center is

$$\varphi(r) = \frac{2\pi\sqrt{r^2+f^2}}{\lambda} \qquad (1)$$

where λ is the wavelength of the incident light in free space. For example, the relationship between φ and r is plotted in Figure 2b for a metalens with a focal length of $f=2.5$ μm and an operational wavelength of $\lambda=676$ nm (see sample **A** in Table 1). The solid line is the required phase shift wrapped by 2π, and the dots indicate the phase shifts provided by the nano-antennas.

Figure 2c shows the results of a full-wave three-dimensional simulation obtained for sample **A** from a commercial finite element method solver (COMSOL Multiphysics). In our simulation, the geometry of the metalens model is taken directly from the actual images obtained from the field emission scanning electron microscopy of the fabricated samples. The permittivity of gold is taken from the interpolated experimental data,[19] which is consistent with the data obtained directly from spectroscopic ellipsometry of our thin-film gold samples. A refractive index of 1.5 is taken for the glass substrate.

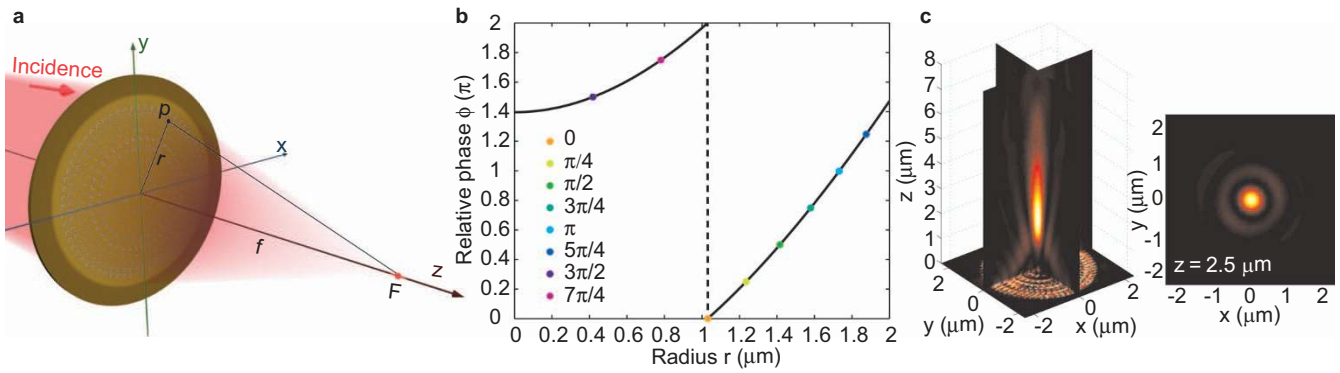

Figure 2 Design principles of the metalenses. (**a**) An illustration of the complementary nano-antennas forming a circular metalens in a plane which focuses light at a focal point *F*. *P* is an arbitrary individual nano-antenna at radius *r* which contributes to the light convergence. All light scattered by such nano-antennas should have constructive interference at *F*. (**b**) The solid curve shows the required phase change at the surface *vs.* the distance to the center of the lens, and the dots show the phase that can be actually provided by the designed complementary plasmonic nano-antennas. The different colors of the dots indicate the phase changes provided by different designs. (**c**) The intensity profiles of the cross-polarized scattered light at the transmission side of sample **A** (Table 1). The data are obtained from the full-wave FEM simulations. (**c**, left panel) Pseudo-color E-field intensity maps depicted on two orthogonal cross-section planes (the *xz*- and *yz*-planes). Both planes intersect at the optical axis of the metalens. (**c**, right panel) E-field intensity mapped on the other cross-section plane (the *xy*-plane) that goes through the focal point; the cross-section is parallel to the surface of the metalens (i.e., perpendicular to the optical axis). FEM, finite element method.

doi:10.1038/lsa.2013.28

Table 1 Design parameters of the fabricated metalens samples

Samples	A	B	C
Focal length at 676 nm f (μm)	2.5	5	7
Radius r (μm)	2	3.5	4.7
Numerical aperture (NA) at 676 nm	0.62	0.57	0.56
Number of nano-antennas	349	1067	1768

RESULTS AND DISCUSSION

The samples are milled in a 30-nm-thick gold film using a focused ion beam. The initial metal film is deposited on a glass substrate with electron-beam vapor deposition. Three different metalens designs are fabricated on the same glass substrate to facilitate characterization. The parameters for the designs are shown in Table 1. Figure 3a shows a field emission scanning electron microscopy image of sample **A**. Note that the focal lengths are designed for a wavelength of 676 nm, and the thicknesses of the samples are only about 1/22 of the operational wavelength.

The schematic of the experimental setup is shown in Figure 3b and is similar to the setup used in Ref. 6. The cross-polarized light intensity is measured using a conventional optical microscope with a 100× objective lens (Numerical aperture=0.75, Working distance=0.98 mm) on the transmission side. The stage resolution along the vertical direction (z-axis) is 0.5 μm, and the depth of focus of our optical system is approximately 0.5 μm, which is sufficient for our measurements.

The sample under test is mounted on the microscope stage with the metalens side up. The sample is then illuminated from the substrate side with a linearly polarized Ar/Kr laser in CW mode. Uniform illumination is ensured by using an incident beam diameter that is orders of magnitude larger than the diameter of a given lens under test. The transmission images from the samples are recorded by a CCD camera. A pair of perpendicular polarizers is placed in the path, one before the sample and the second before the CCD camera, to ensure that only cross-polarized light is collected in the measurement and to eliminate any possible co-polarized background light. As our full-wave simulations of the actual lenses (with experimentally-fit geometries and material constants) prove, the metalenses do not produce any significant cross-polarized stray light; for that reason, there is almost no light capable of distorting the intensity profiles obtained by our method.

By changing the height of the stage in increments of 0.5 μm, we can obtain the intensity distribution at different distances from the surface of the metalens on the transmission side. The focal point of the objective lens and the surface of the sample are coincident at z=0, and (x, y)=(0, 0) is the center of the metalens. The insets in Figure 3b show the CCD images obtained from sample **C** at different heights with 676-nm incident light. From the CCD images, three-dimensional intensity distribution profiles of the cross-polarized light are reconstructed.

Our approach is different from that of confocal scanning optical microscopy,[20] which requires scanning in the x and y directions. A conventional microscope is employed here to recreate the spatial distribution of light by approximating the intensity of the cross-polarized light in the immediate vicinity of the metalens focus. This way, the diffraction that affects the shape of the waist of the beam focused by a metalens is recreated well near the microscope image plane. The CCD detector simply maps this resulting, scaled intensity distribution.

In order to verify the experimental results, we extend the analytical model for two-dimensional diffraction lenses[6] to three-dimensional space. In the model, each nano-antenna is represented as a point source emitting light with a phase corresponding to that scattered by the nano-antenna. The electric field from a point source is proportional to the Green's function in three-dimensional space, and the overall profile of a lens is then just the superposition of the electric field from the various electric point sources.[21] Note that only the cross-polarized component is considered in the model.

Figure 4 shows the reconstructed light intensity distributions for cross-polarized light at 676 nm through three different metalens samples on the transmission side. The pseudo-color field maps obtained from simulations and measurements for each design are plotted side-by-side for comparison. We observed that light is strongly focused at the expected position for each design. At their focal planes, the diameters of the focused light spot are approximately on the scale of the operational wavelength. As shown in Figure 5, the retrieved full widths at half maximum of the intensity distribution on the focal planes are approximately 630 nm, 1000 nm and 1090 nm for samples **A**, **B**, and **C**, respectively. The throughput of a lens is defined by the ratio between the power of the cross-polarized light transmitted through the lens and the total power collected by the lens at the illumination side. The typical throughput of our metalenses is on the order of 10%.

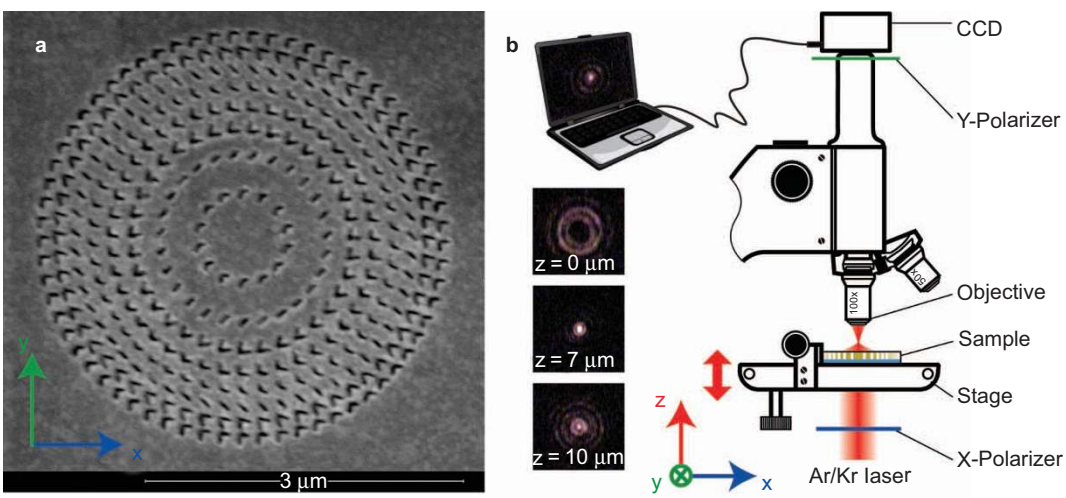

Figure 3 (**a**) A FE SEM image of a fabricated planar plasmonic metalens with a focal length of 2.5 μm at an operational wavelength of 676 nm (sample **A**). (**b**) The schematic of the experimental setup for measuring the light intensity distribution after a metalens sample on the transmission side. FE SEM, field emission scanning electron microscopy.

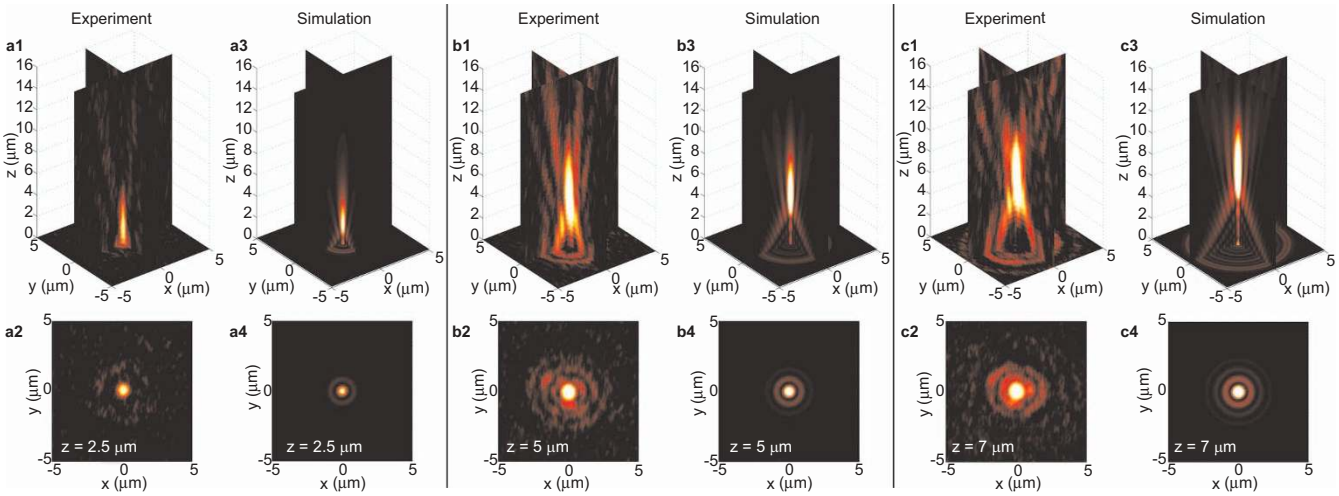

Figure 4 Comparison between the measured and simulated results for three different metalens designs at a wavelength of 676 nm. (**a**) Results for sample **A** designed for a focal length of 2.5 μm. (**b**) Results for sample **B** designed for a focal length of 5 μm. (**c**) Results for sample **C** designed for a focal length of 7 μm. (**a1**, **a2**, **b1**, **b2**, **c1**, and **c2**) Reconstructed cross-polarized light intensity distribution on the transmission side of the metalenses as derived from measurements; (**a3**, **a4**, **b3**, **b4**, **c3**, and **c4**) Simulated results for the same designs. (**a1**, **a3**, **b1**, **b3**, **c1**, and **c3**) Intensity distributions for two cross-sectional planes cutting through the center of the metalens. (**a2**, **a4**, **b2**, **b4**, **c2**, and **c4**) Intensity distribution at the respective focal planes (*z* coordinates are shown on the plots). The *x*–*y* planes in (**a1**), (**b1**), and (**c1**) are at $z=0$ μm. The *x*–*y* planes in (**a3**), (**b3**), and (**c3**) are at $z=0.1$ μm (avoiding the singularity at $z=0$ μm in the simulations). The effect of the depth of focus of the objective lens has been taken into account in the simulations by averaging the intensity data in the *z*-direction within a 0.5-μm window.

We showed in our earlier work that these nano-antennas function well in a relatively wide wavelength range for incident monochromatic light without losing their ability to change the phase of the cross-polarized scattered light.[8] Here, we specifically study the chromatic 'tunability' in the sense that the lens focuses different wavelengths at different positions. For conventional lenses with their typically large, macroscopic focal lengths, this effect is called chromatic aberration (CA) and is usually considered a drawback. In our metalenses, with their ultra-short focal lengths on the order of few micrometers, the absolute shift is comparable to the focal distance itself. To study the extraordinary large CA of the metalenses, we also conduct measurements at incident wavelengths of 531 nm and 476 nm for sample **C**. As shown in Figure 6, the metalens still has a tight light-focusing capability at both wavelengths. The background noise level is higher in the shorter wavelengths because the gold film is more transparent in that range. This could be overcome by using a thicker film or a material that is more metallic in that spectral range, such as silver or aluminum.[22] The measured intensity distributions qualitatively match the simulated profiles. The focal length is shifted to 9 μm and 10 μm at 531 nm and 476 nm, respectively. Such a strong effect gives us a method of controlling the focal length of a metalens by adjusting the incident light wavelength within the entire visible spectrum. By comparing the calculated focal shift of an equivalent, conventional dielectric lens with the shift obtained from our metalens experiments, we conclude that the wavelength-tunable shift in metalenses could be at least *an order of magnitude higher* than that in an equivalent conventional dielectric lens (note that the Fresnel zone plates have the same large CA as the metalenses). While it is hard to have such dynamic control with conventional dielectric lenses because the effect is rather small there, the extraordinarily large CA from metalenses could open up interesting and useful opportunities for novel applications.

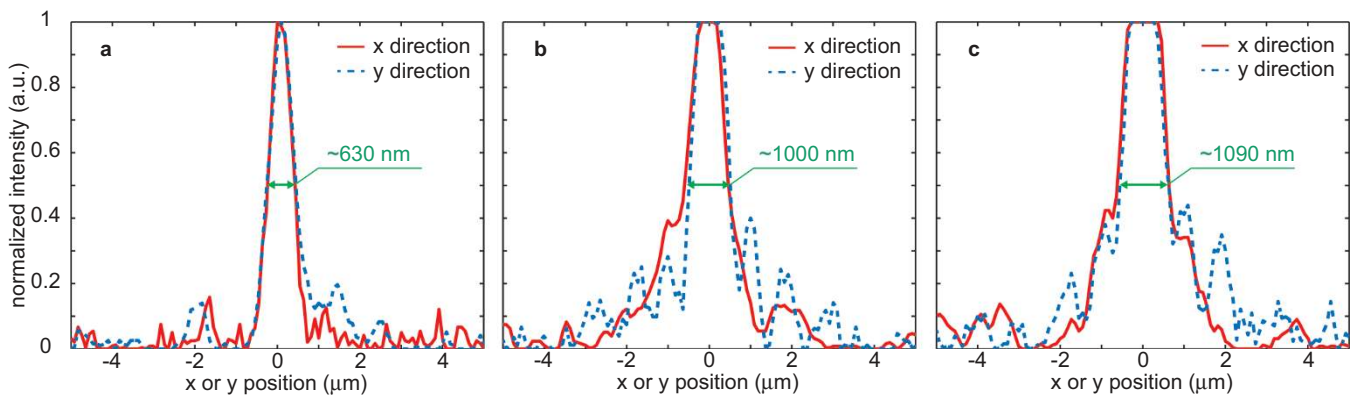

Figure 5 Measured cross-polarized light intensity distribution on the focal plane for (**a**) sample **A**, (**b**) sample **B**, and (**c**) sample **C** along the $y=0$ (red solid curves) and $x=0$ (blue dashed curves) axes. The intensity distribution is normalized to the maximum intensity point in each curve. The retrieved FWHM for each sample is noted in the plots. Note that there are flat peaks in (**b**) and (**c**) because the intensity is so large in the center of the focus that it is out of the CCD response range. Thus the actual FWHM values will be smaller than those noted here. FWHM, full width at half maximum.

doi:10.1038/lsa.2013.28

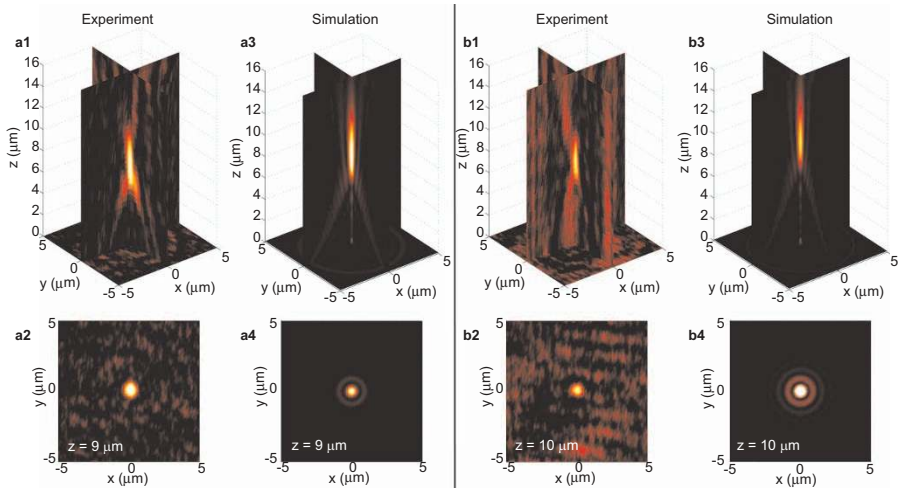

Figure 6 Experimental and simulated results for sample **C** at an incident wavelength of (**a**) 531 nm and (**b**) 476 nm. (**a1**, **a2**, **b1**, and **b2**) Cross-polarized light intensity distributions on the transmission side reconstructed from measurements. (**a3**, **a4**, **b3**, and **b4**) Simulated results under the same conditions. (**a1**, **a3**, **b1**, and **b3**) Intensity distributions for two cross-sectional planes cutting through the center of the metalens. (**a2**, **a4**, **b2**, and **b4**) Intensity distribution at the respective focal planes (*z* coordinates are shown on the plots). The *x*–*y* planes in (**a1**) and (**b1**) are at $z=0$ μm. The *x*–*y* planes in (**a3**) and (**b3**) are at $z=0.1$ μm (avoiding the singularity at $z=0$ μm in the simulations). The effect of the depth of focus of the objective lens has been taken into account in the simulations by averaging the intensity data in *z*-direction within a 0.5-μm window.

Because of the specific symmetry of the nano-antenna building blocks in our design (the last four nano-antennas are identical to the first four nano-antennas upon 90° clockwise rotation), changing the linear polarization of the incident light from *x*-polarized to *y*-polarized creates just an additional π phase shift of the cross-polarized scattered light. This is equivalent to exchanging the first four nano-antennas with the last four (1 and 5 exchange, 2 and 6 exchange, *etc.*). Therefore, the performance of the metalenses should not suffer due to such a polarization change, and we have successfully verified this prediction in our experiments.

CONCLUSIONS

We experimentally demonstrate *x*-/*y*-polarization-independent, ultra-thin and planar metalenses with extraordinarily strong focusing abilities such that the focal spot sizes are larger but still comparable to the wavelength. The lenses are comprised of concentrically arranged, complementary plasmonic nano-antennas (nano-voids) milled in a 30-nm-thick gold film. The nano-voids provide discrete phase shifts ranging from 0 to 2π for cross-polarized scattered light. The Babinet-inverted design greatly increases the signal-to-noise ratio to typically more than 20 times higher than that of previous metallic nano-antenna designs. A particular operational wavelength for our metalenses could be chosen within the entire visible spectral range. This type of metalens is extremely small (a few micrometers in size) and thin (much smaller than the wavelength), and it is easy to design the focal length to be on the order of the operational wavelengths. Thus, $f=2.5$ μm is achieved experimentally with a 4-μm-diameter metalens. We also demonstrate a wavelength-controllable focal length using one of our samples; as our lenses exhibit an extraordinarily large chromatic aberration in comparison with conventional lenses, the optical characterization of this sample confirms that switching the incident wavelength from 676 to 476 nm changes the focal length from 7 to 10 μm. Thus such lenses can spatially separate light at different wavelengths within small, micrometer-scale areas. On top of providing planar, ultra-thin lenses, we also expand the functional space of metalenses by turning them into easy-to-tune elements of future photonics.[23] All these features are advantageous for fabricating on-chip or fiber-embedded optical devices, including nano-photonic couplers, ultra-thin objectives, and micrometer-scale light concentrators.

ACKNOWLEDGMENTS

This work is partially supported by Air Force Office of Scientific Research grant FA9550-12-1-0024, U.S. Army Research Office grant 57981-PH (W911NF-11-1-0359 and grant "Flat photonics with metasurfaces"), and NSF grant DMR-1120923. A V Kildishev is supported by the AFRL Materials and Manufacturing Directorate Applied Metamaterials Program with UES, Inc. S Ishii would like to acknowledge the Japan Society for the Promotion of Science Postdoctoral Fellowships for Research Abroad. The authors acknowledge Dr A S Lagoutchev for valuable discussions and Dr M D Thoreson for help with manuscript preparation.

1 Huang FM, Kao TS, Fedotov VA, Chen Y, Zheludev NI. Nanohole array as a lens. *Nano Lett* 2008; **8**: 2469–2472.
2 Rogers ET, Lindberg J, Roy T, Savo S, Chad JE *et al*. A super-oscillatory lens optical microscope for subwavelength imaging. *Nat Mater* 2012; **11**: 432–435.
3 Verslegers L, Catrysse PB, Yu Z, Fan S. Planar metallic nanoscale slit lenses for angle compensation. *Appl Phys Lett* 2009; **95**: 071112.
4 Lin L, Goh XM, McGuinness LP, Roberts A. Plasmonic lenses formed by two-dimensional nanometric cross-shaped aperture arrays for Fresnel-region focusing. *Nano Lett* 2010; **10**: 1936–1940.
5 Gao H, Hyun JK, Lee MH, Yang JC, Lauhon LJ *et al*. Broadband plasmonic microlenses based on patches of nanoholes. *Nano Lett* 2010; **10**: 4111–4116.
6 Ishii S, Kildishev AV, Shalaev VM, Chen KP, Drachev VP. Metal nanoslit lenses with polarization-selective design. *Opt Lett* 2011; **36**: 451–453.
7 Yu N, Genevet P, Kats MA, Aieta F, Tetienne JP *et al*. Light propagation with phase discontinuities: generalized laws of reflection and refraction. *Science* 2011; **334**: 333–337.
8 Ni X, Emani NK, Kildishev AV, Boltasseva A, Shalaev VM. Broadband light bending with plasmonic nanoantennas. *Science* 2012; **335**: 427.
9 Kats MA, Genevet P, Aoust G, Yu N, Blanchard R *et al*. Giant birefringence in optical antenna arrays with widely tailorable optical anisotropy. *Proc Natl Acad Sci USA* 2012; **109**: 12364–12368.
10 Sun S, He Q, Xiao S, Xu Q, Li X *et al*. Gradient-index meta-surfaces as a bridge linking propagating waves and surface waves. *Nat Mater* 2012; **11**: 426–431.
11 Aieta F, Genevet P, Yu N, Kats MA, Gaburro Z *et al*. Out-of-plane reflection and refraction of light by anisotropic optical antenna metasurfaces with phase discontinuities. *Nano Lett* 2012; **12**: 1702–1706.
12 Genevet P, Yu N, Aieta F, Lin J, Kats MA *et al*. Ultra-thin plasmonic optical vortex plate based on phase discontinuities. *Appl Phys Lett* 2012; **100**: 013101–013103.

13 Larouche S, Smith DR. Reconciliation of generalized refraction with diffraction theory. *Opt Lett* 2012; **37**: 2391–2393.
14 Huang L, Chen X, Mühlenbernd H, Li G, Bai B *et al*. Dispersionless phase discontinuities for controlling light propagation. *Nano Lett* 2012; **12**: 5750–5755.
15 Kang M, Feng T, Wang HT, Li J. Wave front engineering from an array of thin aperture antennas. *Opt Express* 2012; **20**: 15882–15890.
16 Hu D, Wang X, Feng S, Ye J, Sun W *et al*. Ultrathin terahertz planar lenses. arXiv:1206.7011 [physics.optics], 2012.
17 Chen X, Huang L, Mühlenbernd H, Li G, Bai B *et al*. Dual-polarity plasmonic metalens for visible light. *Nat Commun* 2012; **3**: 1198.
18 Aieta F, Genevet P, Kats MA, Yu N, Blanchard R *et al*. Aberration-free ultrathin flat lenses and axicons at telecom wavelengths based on plasmonic metasurfaces. *Nano Lett* 2012; **12**: 4932–4936.
19 Johnson PB, Christy RW. Optical constants of the Noble metals. *Phys Rev B* 1972; **6**: 4370–4379.
20 Verslegers L, Catrysse PB, Yu Z, White JS, Barnard ES *et al*. Planar lenses based on nanoscale slit arrays in a metallic film. *Nano Lett* 2008; **9**: 235–238.
21 Ishii S, Shalaev VM, Kildishev AV. Holey-metal lenses: sieving single modes with proper phases. *Nano Lett* 2012; **13**: 159–163.
22 Boltasseva A, Atwater HA. Low-loss plasmonic metamaterials. *Science* 2011; **331**: 290–291.
23 Kildishev AV, Boltasseva A, Shalaev VM. Planar Photonics with Metasurfaces. *Science* 2013; **339**: DOI: 10.1126/science.1232009